Pyrite contact twins

Yves Moëlo, Massimo Nespolo, François Farges

STRUCTURAL SCIENCE
CRYSTAL ENGINEERING
MATERIALS

ISSN: 2052-5206
journals.iucr.org/b

Pyrite contact twins

Yves Moëlo, Massimo Nespolo and François Farges

Acta Cryst. (2023). B**79**, 32–45

STRUCTURAL SCIENCE
CRYSTAL ENGINEERING
MATERIALS

ISSN 2052-5206

Pyrite contact twins

Yves Moëlo,[a] Massimo Nespolo[b]* and François Farges[c]

[a]Nantes University, CNRS, Institut des Matériaux Jean Rouxel, IMN, Nantes, F-44000, France, [b]Université de Lorraine, CRNS, CRM2, Nancy, France, and [c]Muséum National d'Histoire Naturelle (MNHN), CNRS, IMPMC, Paris, France. *Correspondence e-mail: massimo.nespolo@univ-lorraine.fr

Received 10 July 2022
Accepted 6 December 2022

Edited by M. Dusek, Academy of Sciences of the Czech Republic, Czech Republic

Keywords: pyrite; contact twin; morphology; merohedry; reticular merohedry; iron cross twin; spinel twin.

Two examples of contact twins in pyrite from Peru are described. The first one, from Pasto Bueno ore deposit, shows the pyritohedron {120} as principal form, accompanied by the {111} octahedron and {100} cube as secondary forms, giving a lenticular aspect. (111) is the composition plane, and the twin operation is any one of the three binary axes ⟨110⟩ within this plane. The second one (unknown ore deposit) presents two forms, the octahedron {111} and the pyritohedron {120}; the two crystals in the twin are elongated along [101] and [011], respectively, producing a V profile. It is a reflection twin where the twin plane (110) coincides with the composition plane. These twins are by merohedry. Another contact twin is known in the literature, reported by Gaubert [*Bull. Soc. Fr. Minéral. Cristallogr.* (1928), **51**, 211–212] who described it as a spinel twin, *i.e.* a reflection twin with twin and composition plane (111); here it is shown that it is actually a rotation twin in which the twin operation is a 180° rotation about any of the three equivalent directions ⟨211⟩, contained in the (111) composition plane. The occurrence of these twins as well as the doubtfulness of the spinel twin in pyrite shows a direct relationship with the structural interpretation based on the pseudo-symmetry of the crystallographic orbits.

1. Introduction

Despite its abundance in Nature, pyrite presents only one common twin, generally represented by the 'iron cross' twin (Fig. 1). It corresponds to a penetration twin of two 'pyritohedra', *i.e.* pentagon-dodecahedra of the {120} form, where the twin operation is a fourfold rotation about [001]. Twinning is by merohedry. Sella (1858) reported two twins from Traversella (Piedmont, Italy). The first one (Fig. 2) corresponds to an overgrowth of small pyritohedra on a bigger pyritohedron. Every secondary (small) pyritohedron is located on an edge of the bigger pyritohedron (corresponding to a face of the cube); the twin operation is a twofold rotation

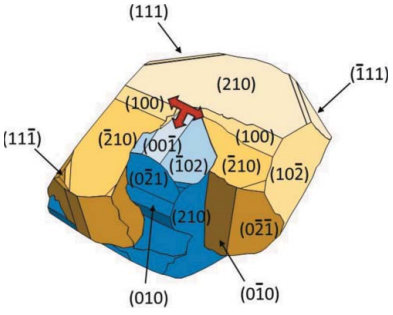

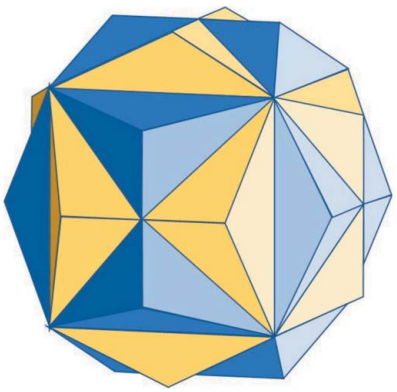

Figure 1
'Iron cross' twin of pyrite.

about [110]. Sella considers this twin as a penetration twin, *i.e.* a peculiar case of iron cross twin. Nevertheless, there is no interpenetration of the twinned crystals, as the small pyritohedra apparently grow in a second step on the passive surface of the pre-existing big one. It would be better to consider such a twinning as a special case of overgrowth twinning. The second twin (Fig. 3) is clearly a contact twin, as indicated by Sella (1858). In the two crystals, the main faces are those of the octahedron (common to the two crystals), combined with minor faces of the pyritohedron (specific to each crystal). (110) is the composition plane, acting as a twin plane.

A second reflection twin in pyrite, also exceptional, is the spinel twin (Palache *et al.*, 1944), *i.e.* a contact twin by reticular merohedry, with (111) as a twin and composition plane; the twin index is 3. It was first observed by Goldschmidt & Nicol (1904) in the French Creek deposit (Pennsylvania, USA), as two twinned octahedra (Fig. 4). A second occurrence from Rif massif (northern Morocco), was described by Gaubert (1928) as corresponding to two twinned cuboctahedra (Fig. 5).

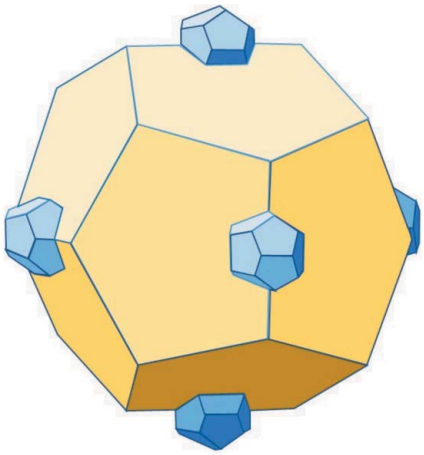

Figure 2
Overgrowth penetration twin from Traversella, after Fig. 65 of Sella (1858).

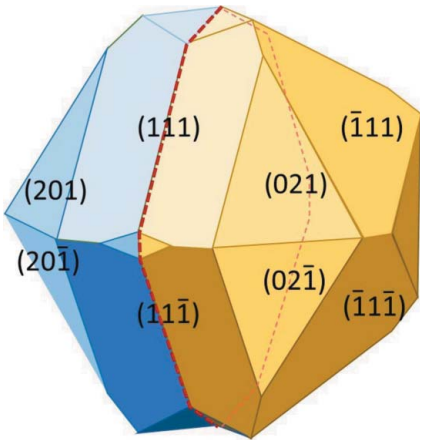

Figure 3
Contact twin from Traversella (Sella, 1858). Red dashed line is a trace of the (110) composition plane acting as a twin plane.

The numerous 'twins' described by Smolař (1913) and reproduced by Goldschmidt (1920), clearly correspond to random interpenetrations of striated cubes (called *triglyph pyrite*, because the striations are reminiscent of the vertically channelled tablets of the Doric frieze in classical architecture). From none of Smolař's 70 figures does it seem possible to derive the orientation of one crystal from that of the other through simple isometries that would correspond to a reasonably low twin index, even considering the possibility of hybrid twinning (Nespolo & Ferraris, 2006).

The present study describes two new examples of pyrite contact twinning, as well as the structural rationale for their occurrence. The first sample (CT1) comes from Pasto Bueno ore deposit (Áncash, Peru). It belonged to an old mineral collection ('G. Palix'), and was provided to one of us (Y.M.) by A. Martaud, a French mineral dealer and collector. The

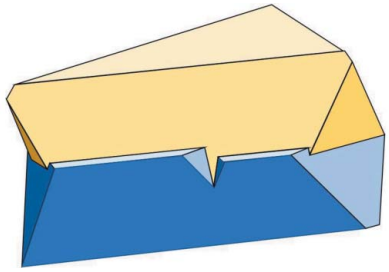

Figure 4
The spinel twin of pyrite, according to Fig. 4 and Table XVI of Goldschmidt & Nicol (1904).

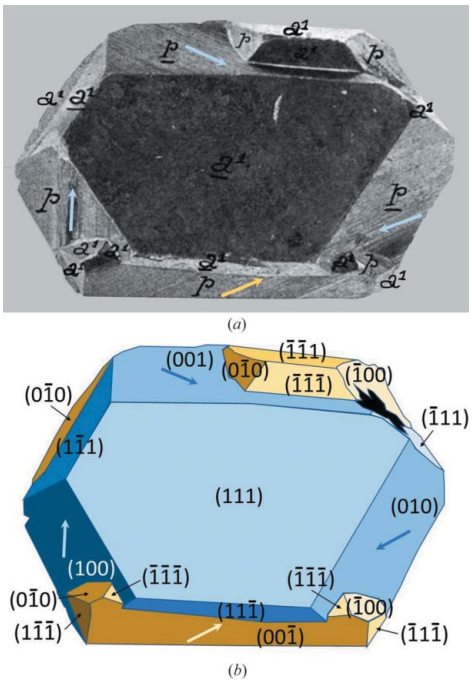

Figure 5
'Spinel twin' of Gaubert (1928): (*a*) photo and (*b*) scheme. Arrows are parallel to striations on cube faces and oriented with their head closer to the central ternary axis.

second sample (CT2) also comes from Peru, without any precision, and was acquired (Y.M.) in a mineralogical exhibition. It was also possible to re-examine Gaubert's sample, archived in the mineralogical collection of the French Museum of National History [MNHN (in French); inventory No. 128.195]. It turns out that this sample does not correspond to the spinel law but to a twin never reported before, which we propose to name the Gaubert twin, according to its first description.

2. Twin study: protocol

The morphological examination has been the benchmark of the investigation of crystals for centuries (Story-Maskelyne, 1895). With the automation of the data collection from X-ray diffractometers, the importance of the morphological investigation has began to be overlooked. This is a serious problem in particular for the study of twinned crystals.

For a complete characterization of twins, information on different scales is necessary.

(*a*) On the macroscopic scale, based on the morphological investigation.

(*b*) On the reticular level, to characterize the sublattice common to the twinned individuals.

(*c*) On the structural level, to identify the substructure that is, exactly or approximately, restored (*i.e.* mapped from one individual to the adjacent one) by the twin operation(s).

From the morphological viewpoint, the characterization of a twinned crystal requires the identification of the composition surface and the twin operation(s). The composition surface can be a plane, in the case of contact twins, or an irregular surface, in the case of penetration twins (Friedel, 1904). For contact twins, several possibilities exist.

(i) In the case of reflection twins, the twin plane can be parallel to the composition plane or differently oriented;

(ii) In the case of rotation twins, the twin operation can be a binary rotation or a rotation of higher order;

(iii) If the twin operation is a binary rotation, the twin axis can be contained in the composition plane or normal to it; one speaks of parallel hemitropy and normal hemitropy respectively (from the Greek $h\mu\iota$ 'half' and $\tau\rho o\pi\acute{\iota}\alpha$ 'to turn') (Haüy, 1801; see also Bravais, 1851). This categorization has been criticized by Friedel (1926), but its usefulness has been recently reported by Nespolo & Souvignier (2017).

In the following sections we present a detailed morphological investigation of pyrite contact twins, followed by the structural study. This is accompanied by the construction of the twin (chromatic) point group, expressing the symmetry of the whole twinned edifice, and the reticular interpretation, *i.e.* the (sub)lattice common to the individuals and the twin index, expressing the (reciprocal of the) degree of lattice overlap obtained by the twin operation. The reader less familiar with the procedure will find all the details in Nespolo (2015, 2019).

A twin operation t maps the orientation X_1 of a crystal taken as reference to the orientation X_2 of a second crystal of the twin. The point groups of the two crystals, $\mathcal{H}_1$ and $\mathcal{H}_2$, are of the same type but their symmetry elements are, in general, differently oriented in space. $\mathcal{H}_1$ and $\mathcal{H}_2$ are conjugated under the twin operation

$$X_2 = tX_1;\ \mathcal{H}_2 = t\mathcal{H}_1t^{-1}. \tag{1}$$

The intersection group $\mathcal{H}^*$ contains the symmetry operations common to $\mathcal{H}_1$ and $\mathcal{H}_2$ in their respective orientations; it is a subgroup of both $\mathcal{H}_1$ and $\mathcal{H}_2$:

$$\mathcal{H}^* = \mathcal{H}_1 \cap \mathcal{H}_2. \tag{2}$$

The dichromatic twin point group $\mathcal{K}^{(2)}$, which represents the point group of the whole twinned edifice, is obtained by extending $\mathcal{H}^*$ through a point group {1,t} containing the identity and the twin operation t[1]:

$$\mathcal{K}^{(2)} = \mathcal{H}^* \times \{1, t\};\ t = (\mathbf{W}). \tag{3}$$

where **W** is the matrix representation of the twin operation, which contains only a linear part, without any translation. $\mathcal{K}^{(2)}$ is a dichromatic group: colour-preserving operations are symmetry operations leaving invariant both individuals of the twin; they compose the intersection subgroup $\mathcal{H}^*$. Colour-exchanging operations, obtained as $\mathcal{H}^* \times t$, are twin operations that map the two individuals onto each other. For a p-individual twin, the twin point group $\mathcal{K}^{(p)}$ is polychromatic of chromaticity p and the set extending the intersection subgroup $\mathcal{H}^*$ contains $p-1$ twin operations: $\{1, t_1, t_2, \ldots, t_{p-1}\}$ (Nespolo, 2019).

Pyrite is cubic hemihedral, point group $\mathcal{H} = m\bar{3}$. The iron cross twin is obtained by a fourfold rotation about ⟨001⟩. The twin point group and the twin law are therefore immediately established:

$$\begin{aligned}\mathcal{H}^* = 2/m\bar{3};\ \mathcal{K}^{(2)} = 2/m\bar{3} \times \left\{1, 4_{[001]}\right\} = m\bar{3} \cup \Big\{ & 4'^{+}_{[001]}, 4'^{-}_{[001]}, \bar{4}'^{+}_{[001]}, \\ & \bar{4}'^{-}_{[001]}, 4'^{+}_{[010]}, 4'^{-}_{[010]}, \bar{4}'^{+}_{[010]}, \bar{4}'^{-}_{[010]}, 4'^{+}_{[100]}, 4'^{-}_{[100]}, \bar{4}'^{+}_{[100]}, \bar{4}'^{-}_{[100]}, 2'_{[110]}, \\ & 2'_{[1\bar{1}0]}, 2'_{[101]}, 2'_{[10\bar{1}]}, 2'_{[011]}, 2'_{[01\bar{1}]}, m'_{[110]}, m'_{[1\bar{1}0]}, m'_{[101]}, m'_{[10\bar{1}]}, \\ & m'_{[011]}, m'_{[01\bar{1}]} \Big\} = 4'/m\bar{3}2'/m'\end{aligned} \tag{4}$$

where the first coset is the point group of the crystal, $m\bar{3}$, which is invariant under conjugation by $4_{[001]}$, and the second coset is the twin law, which contains 24 twin operations. The orientation of one individual of the twin can be mapped to that of the other through any of the 24 twin operations contained in the twin law. Therefore, the penetration twin described by Sella (1858) and reproduced in Fig. 2 is nothing other than an iron cross twin showing, instead of two individuals with roughly the same volume, seven individuals (a large central crystal and six small crystals coming out from the edges of two faces of the dodecahedron), corresponding to two orientations. This was realized by Sella himself, who stated (page 333) that if the development of the crystal would have continued, we would obtain a situation similar to that of the twin from Valdieri (another locality in Piedmont, Italy), reproduced in

[1] If the twin operation t is an order higher than 2, then {1,t} is a set. The extension $\mathcal{H}^* \times \{1,t\}$ may result into a group, if it contains all the operations t, $t^2, \ldots, t^n = 1$, otherwise it is a point groupoid. For details, see Nespolo (2019).

Table 1
The four contact twins in pyrite.

Twin	Composition plane	Twin operation identified from the morphological investigation
CT1	{111}	$2_{\langle 110\rangle}$
CT2	{110}	$m_{\langle 110\rangle}$
Gaubert	{111}	180° rotation around $[2\bar{1}\bar{1}]$, $[\bar{1}2\bar{1}]$, or $[\bar{1}\bar{1}2]$
Spinel	{111}	(111) as mirror or $(2n+1)60°$ rotation around [111]

his Fig. 65, but with only one pyritohedron: {120}. The pyrite twin from Valdieri is a penetration twin of two individuals of roughly the same volume, each composed by two pyritohedra: {120} and {340}. Removing the {340} form from the Valdieri twin would result in the classical iron cross twin.

Table 1 summarizes the results of the morphological investigations detailed in the following sections. For first two contact twins, labelled CT1 and CT2 hereafter, the twin operations are symmetry operations of the lattice. Therefore, twinning is by merohedry and the twin point group is the same as that of the iron cross twin [equation (4)]. The difference between these twins is that:

(i) the iron cross twin is a penetration twin, whereas the two others are contact twins,

(ii) CT1 and CT2 differ by their composition plane.

The information about the composition plane is clearly of paramount importance and it requires a morphological investigation of the sample; the twin law alone cannot uniquely define the twin. Unfortunately, in many cases the morphological study of a twinned crystal is skipped by the investigators, who proceed immediately with the structural study, so that a fundamental piece of information is missing in their reports.

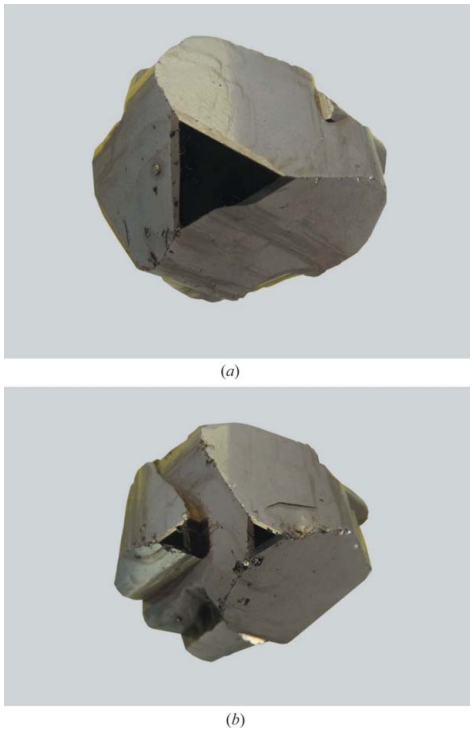

Figure 6
Photographs of the contact twin from Pasto Bueno: (*a*) top view and (*b*) bottom view.

3. Morphological investigation

3.1. Sample CT1

The twin (54 g) has an ellipsoidal shape (top view in Figs. 6 and 7): ∼3.5 cm × 3.2 cm; profile view (Figs. 8 and 9): ∼2.5 cm high], slightly flattened parallel to (111). Pyritohedron faces predominate, octahedron faces are more or less developed, while cube striated faces are less evident. Small additional facets border the triangles of octahedron faces. On one side, one crystal largely overflows the second one, so that its (111) face is adjacent to the (111) face of the other individual

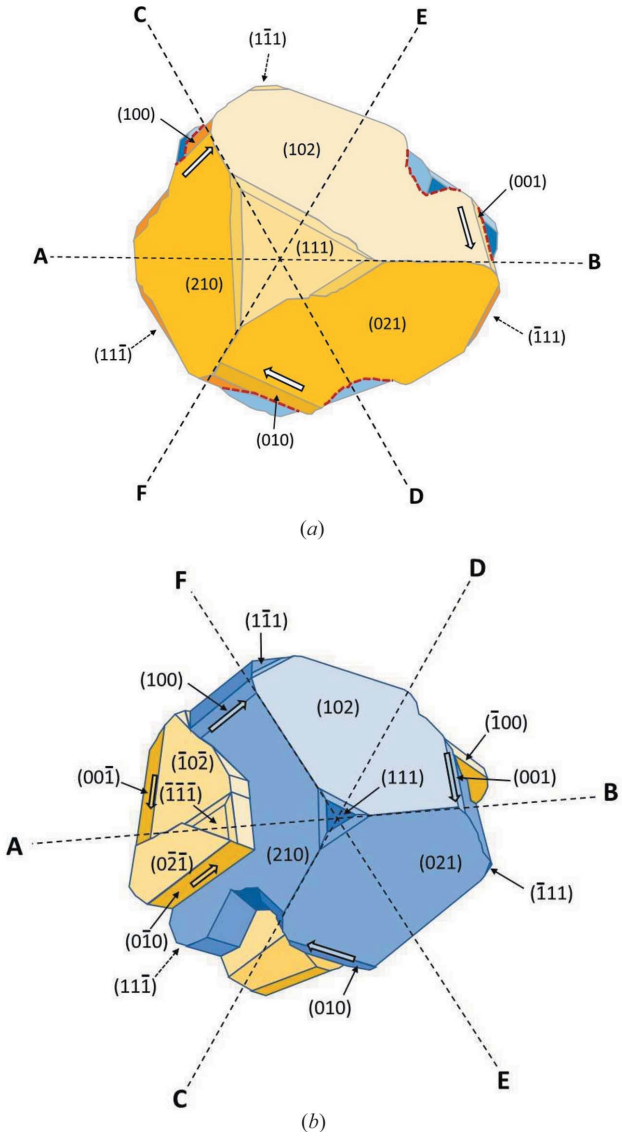

Figure 7
Schemes of the contact twin from Pasto Bueno: top view (*a*) and bottom view (*b*). In accordance with striations, large empty arrows indicate a clockwise rotation around the [111] ternary axis.

[Fig. 7(*b*)]. There is a sinuous contact line between the two crystals (Fig. 8), which imperfectly reproduces the crystal interlinking of the iron cross (Fig. 9).

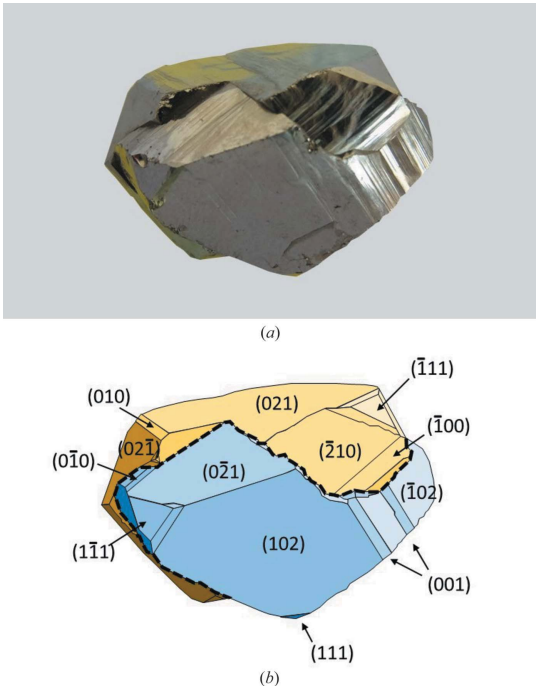

Figure 8
Lateral view according to $E \rightarrow F$ direction: (*a*) photo, (*b*) scheme. Thick dashed line is the twin contact.

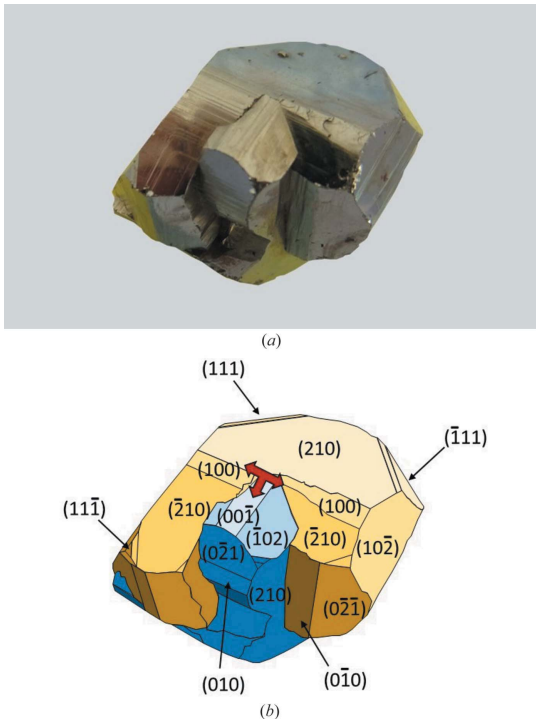

Figure 9
Lateral view according to $C \rightarrow D$ direction: (*a*) photo and (*b*) scheme. Triple red arrow: half iron cross.

The hemihedral symmetry of the structure is reflected in the well known striations on their {100} (cube) and {210} (pyritohedron), either 'positive' (parallel to [001]) or, more rarely, 'negative' (perpendicular to [001]) (Endo & Sunagawa, 1973). Acting on a cuboctahedron with striated cubic faces [Fig. 10(*a*)], the twin operation changes the direction of striations (arrows) in the half bottom part of the cuboctahedron [Fig. 10(*b*)]. This leads to two possible morphological sub-types, according to the clockwise or anticlockwise rotation on the two sides of the twin. Pasto Bueno twin refers to the clockwise sub-type.

According to Grigoriev (1965), the contact between two individuals to form a twinned crystal favours their growth, to give a dissymmetric habit. The best example is that of La Gardette, or Japan twin of quartz, giving flattened prisms within the plane determined by the two ternary axes. Starting from a simple pyrite octahedron, such a twin may induce a flat crystal, without visible striations [Fig. 11(*a*)]. It may be the case of the flat octahedron described by Goldschmidt (1920)

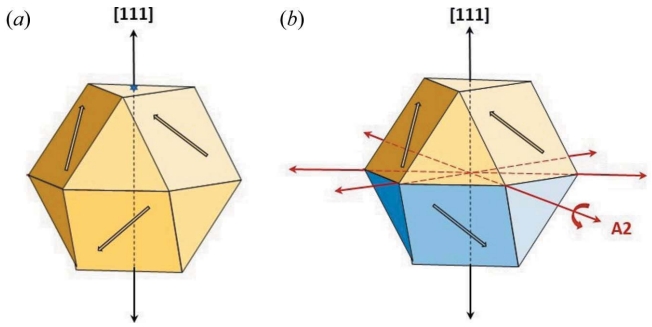

Figure 10
Derivation of contact twin (Pasto Bueno type) starting from a primitive cuboctahedron: (*a*) untwinned crystal and (*b*) twin through 180° rotation around a [110] direction (red arrow) perpendicular to [111] ternary axis. Green arrows indicate striations typical of triglyph pyrite, with their polarity related to [111] ternary axis.

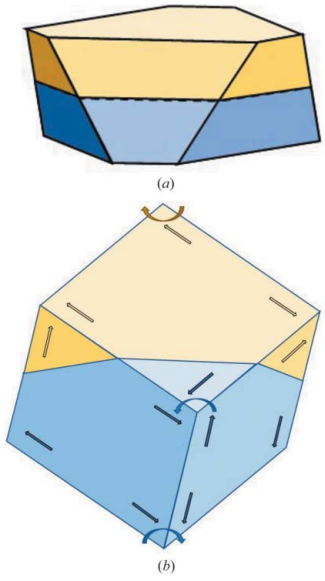

Figure 11
Pasto Bueno twin type: (*a*) starting from an octahedron and (*b*) starting from a cube. The two opposite corners present the same clockwise rotation, according to striations (arrows).

(Fig. 87, Table 107 therein). On the contrary, starting from a simple cube will not induce a dissymmetry, but the striation of cube faces, if present, will reveal the presence of twinning [Fig. 11(*b*)].

As there is a continuity between cube or octahedron faces across the composition plane separating the two crystals, the contact line will respect the primitive (111) surface. This is not the case for the faces of the pyritohedron. It explains the sinuous contact line observed in Pasto Bueno twin (Fig. 8), with partial overgrowth of one crystal on the other one [Fig. 7(*b*)]. According to observations as well as theoretical approaches (Kostov & Kostov, 1999), {111} is the first form of pyrite crystal growth. It was probably the case for Pasto Bueno twin, before the appearance of {100} and {210} forms.

Opposite triangular (111) faces of the two crystals match like in the spinel twin, a reflection twin in which both the twin plane and the composition plane are parallel to (111). As in the case of triglyph pyrite, the striations of the faces of the cube, oblique relatively to the ternary axes, allow us to define clockwise or anticlockwise rotations. The top view [Fig. 7(*a*)] indicates a clockwise rotation of the upper crystal (see large arrows). The same thing applies to the crystal below [Fig. 7(*b*)]. This is incompatible with a mirror reflection, which would map a clockwise onto an anticlockwise one. This twin cannot therefore be explained on the basis of the spinel law.

The incomplete iron cross visible along the contact line [Fig. 9(*b*)] indicates that the twin is obtained through a twin operation among those acting for the iron cross in equation (4). As a mirror is excluded, the twin operation must be a rotation about a direction contained in the (111) composition plane, *i.e.* a twin by parallel hemitropy, with twin operation $2_{\langle 110\rangle}$.

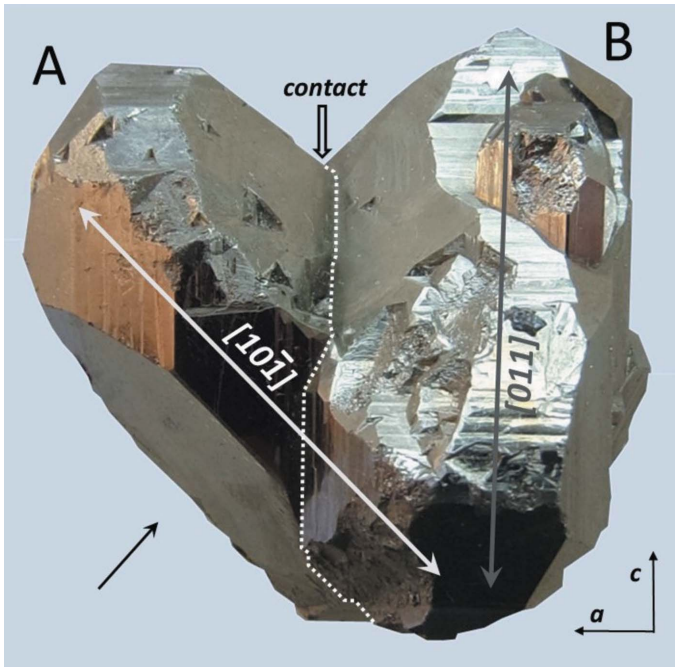

Figure 12
V contact twin from Peru (CT2 sample). Oblique view. A and B are the two twinned individuals. Double-headed arrows are elongation directions.

The directions of the twin elements correspond to the lines *AB*, *CD* and *EF* in Fig. 7. We therefore conclude that this contact twin from Pasto Bueno shares with the spinel twin the composition plane (111) but differs in respect to the twin operations.

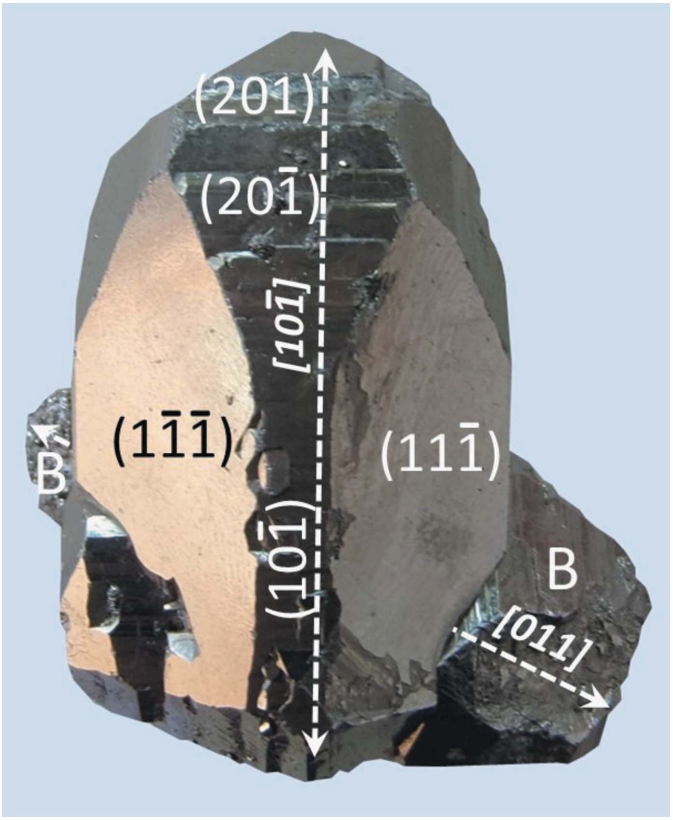

Figure 13
V contact twin. Pseudo-orthorhombic habit of crystal A. Double-headed white arrows: elongation directions.

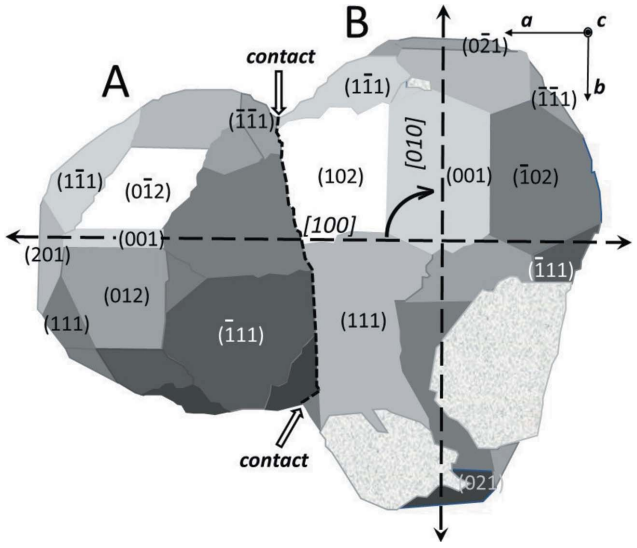

Figure 14
Scheme along *c* of V contact twin, with indication of the twin law according to a 90° rotation around *c* axis. Curved arrow: 90° rotation from [100] to [010] directions (double-headed arrows).

3.2. Sample CT2

In this sample (about 120 g; approximate dimensions 5 cm × 4 cm × 4 cm), two crystals (**A** and **B**) are joined in a V shape (Fig. 12). In the axial setting of one individual (**A**), **A** is elongated along [101] and **B** along [011]. The main faces are those of octahedron and pyritohedron, *i.e.* {111} and {210}, accompanied by smaller cubic faces, {100}. In **A**, the {111} faces parallel to [101] produce a pseudo-orthorhombic habit (Fig. 13).

The observation along the *c* axis (Fig. 14) shows that the orientation of **B** is obtained from that of **A** through a 90° rotation about [001]. As in the case of CT1, twinning is by merohedry. Initially, the composition surface between the two crystals should be the bisector plane (110), as indicated in Fig. 15, ideally taking into account two octahedra. In such an outline, the (110) plane also acts as a twin plane. Nevertheless, due to the strong development of the {120} form, in the final habit only the 90° rotation twin operation is clearly visible. This contact twin relates to the same twin type described by Sella (1858) (Fig. 3). We will see in the structural study that the twin operation should actually be described as a reflection about the (110) plane.

3.3. Re-examination of the Gaubert twin (formerly assigned as 'spinel' twin)

According to Gaubert (1928), this sample (Fig. 5) was collected by R. Ph. Dollfus, professor of biology at the French MNHN, in the alluvium of a river in the Moroccan Rif chain. Despite a thin oxidation film, characteristic striation of triglyph pyrite is visible on cube faces. In the three faces of the top crystal [in blue, Fig. 5(*b*)], this striation indicates a clockwise rotation. One upper (100) face of the lower crystal clearly shows an anticlockwise rotation [in yellow, Fig. 5(*b*)]. As a consequence, on the other side of the twin, cube faces of the lower crystal show a clockwise rotation. This is incompatible with the spinel twin, where the (111) composition plane, acting as twin plane, reverses the direction of rotation (Fig. 16).

Like in the Pasto Bueno twin, this twin implies a binary axis within the (111) contact plane. But in this case it corresponds

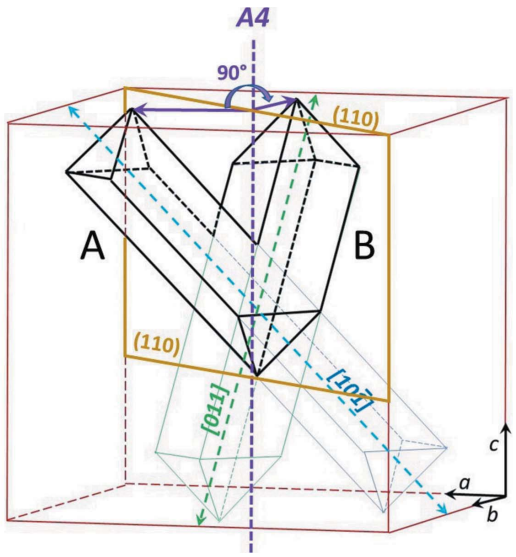

Figure 15
Ideal scheme of the V twin starting from two elongated octahedra.

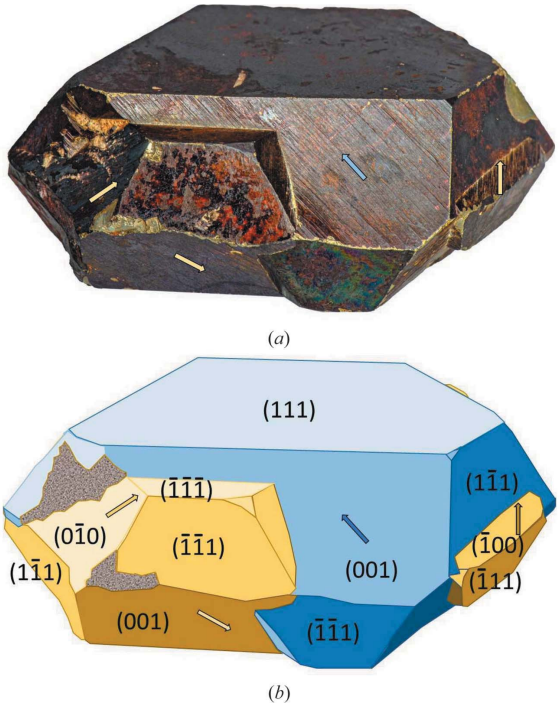

Figure 16
Oblique view of the Gaubert twin (*a*), with the indexing on the corresponding drawing (*b*).

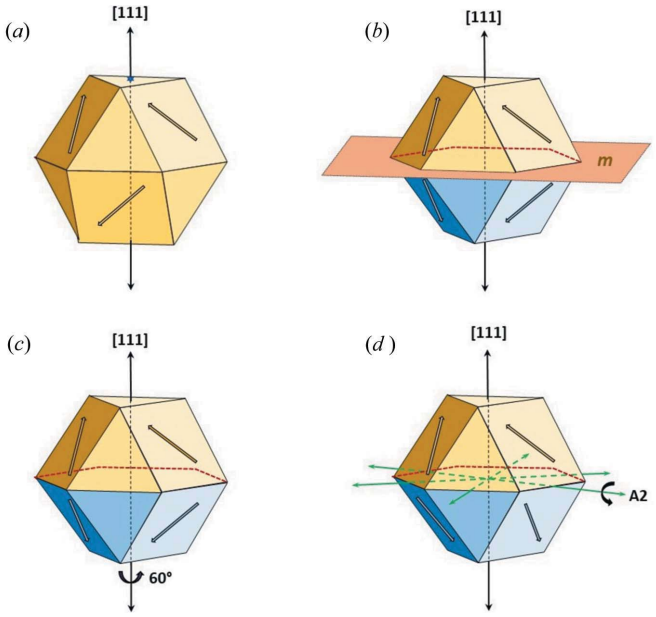

Figure 17
Comparison of the spinel twin and the Gaubert twin, starting from a pyrite cuboctahedron (*a*). The spinel twin with indication of the mirror *m*, or the (2*n*+1)60° rotation around the [111] axis: (*b*) and (*c*), respectively. (*d*) The Gaubert twin according to an 180° rotation about a direction contained in the (111) plane ([2$\bar{1}$1], [$\bar{1}$2$\bar{1}$] or [$\bar{1}\bar{1}$2] – double-headed green arrows).

to one of three equivalent directions within the (111) plane: $[2\bar{1}\bar{1}]$, $[\bar{1}2\bar{1}]$ or $[\bar{1}\bar{1}2]$. In Fig. 17, the Gaubert twin is compared with the spinel twin, starting with a cuboctahedron. On cube faces, striation directions indicating pyrite hemihedry have been symbolized by arrows. In the primitive form [Fig. 17(*a*)], relatively to a given ternary axis, a clockwise rotation faces an anticlockwise one. Relative to the (111) plane, a cube face of the top crystal is in front of an octahedral face of the bottom crystal. In the spinel twin, where either a mirror reflection or a $(2n+1)60^\circ$ rotation ($n \in \mathbb{Z}$) act as twin operation [Figs. 17(*b*) and 17(*c*), respectively], there is a change in the direction of rotation. In the contact twin of the Pasto Bueno type [Fig. 17(*d*)], the only change relatively to Fig. 17(*a*) is the same clockwise rotation for the top and bottom crystals. We can conclude that this is a new type of contact twin, for which we propose the name *Gaubert twin*, according to its first description.

To find the intersection subgroup we first describe the structure in a setting in which the twin axis is along a basis vector. A suitable basis is obtained by $\mathbf{a}-\mathbf{c}$, $-\mathbf{a}+\mathbf{b}$, $\mathbf{a}+\mathbf{b}+\mathbf{c}$, which leads to an hP unit cell with parameters $a = 2^{1/2}a_{\rm pyr}$, $c = 3^{1/2}a_{\rm pyr}$. The composition plane in this setting becomes (001). The intersection subgroup is $\bar{3}$ and the twin operation is a twofold rotation about [120], so that the twin point group is $\bar{3}12'/m'$. Twinning is by reticular merohedry with twin index 3.

Like in the Pasto Bueno type, there are two sub-types, clockwise or anticlockwise. In euhedral crystals, this twin type cannot be distinguished from the spinel twin if only (111) and (100) forms (without striations) are present. The question remains whether the twins described by Goldschmidt & Nicol (1904) are really spinel twins, or, on the contrary, Gaubert twins. As we are going to show in the next section, the spinel twin would results in a larger strain at the composition plane, which likely results in a lower occurrence probability. Owing to the small size (1–2 mm) of twinned crystals examined by Goldschmidt & Nicol (1904), it would be possible to investigate them by a non-destructive X-ray study, to unequivocally assign them to either type.

4. Structural study: general principles

At the atomic scale, the characterization of a twin is based on the pseudo-symmetry of the crystallographic orbits. The infinitely many operations of a space group, acting on the finitely many atoms contained in the asymmetric unit, produce a finite number of crystallographic orbits, each of which is infinitely extended (the surface of the crystal being, as usual, considered as a defect). Each crystallographic orbit has an eigensymmetry $\mathcal{E}$ which may coincide with the space group $\mathcal{G}$ of the crystal or be a supergroup of it. One speaks, respectively, of characteristic and non-characteristic orbits. For non-characteristic orbits, $\mathcal{E}$ contains additional operations with respect to $\mathcal{G}$, of which one or more may have the same linear part as the twin operation: these are called *restoration operations*. If that is the case, the crystallographic orbit under consideration is mapped without modification in the neighbour crystal of the twin; that orbit crosses without perturbation the interface (commonly known as the *composition surface* in the twin literature). If a significant portion of the crystallographic orbits fulfils this condition, then a significant substructure is not affected by the twin operation and builds up the common substructure of the twin. If this common substructure preserves the coordination polyhedra of a non-molecular structure (Marzouki *et al.*, 2014*a*) or the chemical moiety of a molecular structure (Vijayakumar-Syamala *et al.*, 2022), it may justify the occurrence of a twin on a structural basis. If $\mathcal{E}$ represents only a pseudo-symmetry, then the common substructure undergoes some strains at the interface between two crystals of the twin; as a consequence, the coordination polyhedra (for non-molecular crystals) or the molecule conformation (for molecular crystals) are distorted near the interface.

The degree of pseudo-symmetry of a crystallographic orbit can be evaluated as the distance that an atom of that orbit should be moved by for the eigensymmetry $\mathcal{E}$ of the orbit to increase to a supergroup $\mathcal{E}'$. Specifically, an atom X with coordinates x, y, z under the action of the space group $\mathcal{G}$ of the crystal generates the crystallographic orbit {X}, whose eigensymmetry is $\mathcal{E}$:

$$\mathrm{X} = x, y, z; \{\mathrm{X}\} = \mathcal{G}\mathrm{X}; \mathcal{E}\{\mathrm{X}\} = \{\mathrm{X}\}, \mathcal{E} \supseteq \mathcal{G}. \quad (5)$$

By moving the atom X to a nearby position $\mathrm{X}' = x', y', z'$ the eigensymmetry of the crystallographic orbit is increased to a supergroup $\mathcal{E}'$ of $\mathcal{E}$:

$$\mathrm{X}' = x', y', z'; \{\mathrm{X}'\} = \mathcal{G}\mathrm{X}'; \mathcal{E}'\{\mathrm{X}'\} = \{\mathrm{X}'\}, \mathcal{E}' \supset \mathcal{E} \supseteq \mathcal{G}. \quad (6)$$

The degree of pseudo-symmetry can be estimated by the distance $|\mathbf{u}|$, in Ångströms, corresponding to the shift $(\Delta\mathrm{X}| = (x' - x, y' - y, z' - z)$:

$$|\mathbf{u}| = (\Delta\mathrm{X}|\mathbf{G}|\Delta\mathrm{X})^{1/2}, \quad (7)$$

where $(\Delta\mathrm{X}|$ is a row vector, $|\Delta\mathrm{X})$ its transpose (column vector) and $\mathbf{G}$ is the metric tensor. The tolerance on $|\mathbf{u}|$ cannot be defined *a priori*, because the same value of $|\mathbf{u}|$ does not have the same physical meaning depending on the atomic size. As a 'rule of the thumb' adopted in our previous publications, a value of $|\mathbf{u}|$ lower than the covalent or ionic radius (depending on the nature of the chemical bond) sounds reasonable.

This approach, introduced by Donnay & Curien (1960) and developed by Marzouki *et al.* (2014*b*), has been successfully applied to a number of mineral structures and, very recently, also to a molecular crystal undergoing reversible twinning under compression (Vijayakumar-Syamala *et al.*, 2022). The unfamiliar reader will find all the details in our previous publications (Nespolo & Moëlo, 2019, and references therein).

In a perfectly parallel way to what has already been introduced for point groups [equation (3)], the intersection subgroup $\mathcal{G}^*$ of the space groups $\mathcal{G}_1$ and $\mathcal{G}_2$ in their respective orientations is obtained as:

$$\mathcal{G}^* = \mathcal{G}_1 \cap \mathcal{G}_2 = \mathcal{G}_1 \cap \mathrm{s}\mathcal{G}_1\mathrm{s}^{-1}; \mathrm{s} = (\mathbf{W}, \mathbf{w}), \quad (8)$$

where $(\mathbf{W},\mathbf{w})$ is the matrix-column pair representation of the restoration operation s. The linear part $\mathbf{W}$ must be common to s and t for the crystallographic orbit to contribute to the common substructure. The column part of $\mathbf{w}$ identifies the

Table 2
Splitting of the crystallographic orbits from $Pa\bar{3}$ to $R\bar{3}$ and corresponding approximate pseudo-symmetry in $R\bar{3}m$, a supergroup containing the restoration operation corresponding to the twin operation for both CT1 and CT2 twins.

The values of the covalent radii are taken from Cordero *et al.* (2008). $|\mathbf{u}|/r$ is the ratio of the atomic displacement $|\mathbf{u}|$ [equation (7)] and the covalent radius r. $|\mathbf{u}|$and r are both in Å.

		Description in $Pa\bar{3}$			Description in $R\bar{3}$			Pseudo-symmetry $R\bar{3}m$ **a**, **b**, **c**	
Orbit	Covalent radius r (Å)	Wyckoff position	Site-symmetry group	Fractional atomic coordinates	Wyckoff position	Site-symmetry group	Fractional atomic coordinates	$\|\mathbf{u}\|$	$\|\mathbf{u}\|/r$
Fe	1.32	4*a*	.$\bar{3}$.	0, 0, 0	9*d*	$\bar{1}$	$\frac{1}{2}, \frac{1}{2}, \frac{1}{2}$	0	0
					3*b*	$\bar{3}$.	0, 0, $\frac{1}{2}$	0	0
S	1.05	8*c*	.3.	0.38488, 0.38488, 0.38488	18*f*	1	0.25659, 0.01317, 0.62829	0.62	0.59
					6*c*	3.	$\frac{1}{3}, \frac{2}{3}$, 0.55155	0	0

nature of the operation (rotation or screw-rotation; reflection or glide reflection) and the location of its geometric element with respect to the chosen coordinate system. The intersection subgroup $\mathcal{G}^*$ contains the operations that have the same linear part **W** and a translation part **w** identical modulo a lattice translation. In contrast to point groups, the twin cannot be described by a chromatic space group, because the chromatic operations do not apply to the whole structure but only to a substructure, built by the non-characteristic orbits whose eigensymmetry includes operation(s) whose linear part coincides with the twin operation.

In the coordinate system of pyrite, Fe occupies Wyckoff position 4*a* with site-symmetry group .$\bar{3}$. and fractional atomic coordinates 0, 0, 0, whereas S occupies Wyckoff position 8*c* with site-symmetry group .3. and fractional atomic coordinates x, x, x. We will consider the structure reported by Rieder *et al.* (2007), for which $x = 0.38488$ and $a = 5.416$ Å. The search of pseudo-symmetry is performed with the routine *PSEUDO* (Capillas *et al.*, 2011) at the Bilbao Crystallographic Server (Aroyo *et al.*, 2006).

4.1. CT1 twin

The twin operation is $2_{\langle 110\rangle}$ and the space group of the second individual, $\mathcal{G}_2 = (2_{\langle 110\rangle}|\mathbf{0})\mathcal{G}_1(2_{\langle 110\rangle}|\mathbf{0})$, where **0** is the null translation vector, is $Pb\bar{3}$, the unconventional setting of $Pa\bar{3}$ (Nespolo *et al.*, 2020). We know from the point group analysis that the linear part of the symmetry operations is unchanged under conjugation by $2_{\langle 110\rangle}(\mathcal{H}^* = m\bar{3})$; on the other hand, the translation part is affected by the conjugation relation and the only operations that, under conjugation, differ by a lattice translation are the identity, the inversion and the four operations 3^+, 3^-, $\bar{3}^+$ and $\bar{3}^-$ about one of the four $\langle 111\rangle$ of the cubic lattice. The direction of the threefold axis surviving in the intersection subgroup depends on which of the six operations $2_{\langle 110\rangle}$ is chosen as the conjugating operation, so that one gets four possible intersection subgroups, which differ for the orientation in space of their symmetry elements. These intersection subgroups are conjugated and this justifies the fact that they lead to the same result once the conventional setting, with the threefold axis oriented along [001], is chosen. Let us illustrate the procedure by selecting $2_{[110]}$ as the conjugating operation. The threefold axis surviving in the intersection subgroup is along $[\bar{1}11]$, because the only operations which differ by a lattice translation in $\mathcal{G}_1$ and $\mathcal{G}_2$, besides the identity and the inversion, are

$$3^+_{[\bar{1}11]},\ 3^-_{[\bar{1}11]},\ \bar{3}^+_{[\bar{1}11]} \text{ and } \bar{3}^-_{[\bar{1}11]};$$

the composition plane becomes $(\bar{1}11)$. We also know that the whole lattice is restored (twinning by merohedry). The coordinate system of pyrite is no longer the most suitable one to describe the symmetry of the twin, because the threefold axis surviving in $\mathcal{G}^*$ is along a body diagonal of the cubic cell. To obtain a conventional description of the intersection subgroup a change of basis is necessary: $-\mathbf{a}-\mathbf{c}$, $-\mathbf{b}+\mathbf{c}$, $-\mathbf{a}+\mathbf{b}+\mathbf{c}$; in this setting, the composition plane becomes (001) whereas the twin axis remains [110]. The resulting coordinate system is *hR*, with $a = 2^{1/2}a_{\rm pyr}$ and $c = 3^{1/2}a_{\rm pyr}$ (the lattice nodes centring the *hR* unit cell have coordinates $\bar{1}00$ and $\bar{1}01$, respectively, in the coordinate system of pyrite). In symbols

$$\mathcal{G}^* = \mathcal{G}_1 \cap 2(_{[110]}|\mathbf{0})\mathcal{G}_1(2_{[110]}|\mathbf{0}) = R\bar{3}. \qquad (9)$$

To find the common substructure restored, exactly or approximately, by the twin operation, one has to find the crystallographic orbits whose eigensymmetry is a minimal supergroup of $R\bar{3}$ containing a twofold rotation or screw rotation about $2_{[110]}$. In other words, those crystallographic orbits whose eigensymmetry is at least $R\bar{3}m$ or $R\bar{3}c$.

The matrix–column pair that relates the coordinate systems of the group and of the intersection subgroup includes a shift of the origin by $0, 0, \frac{1}{2}$. This transformation of coordinate system is necessary to compute the splitting of Wyckoff positions (Wondratschek, 1993) from $\mathcal{G}$ to $\mathcal{G}^*$. In the setting of $R\bar{3}$, the Fe 4*a* orbit of $Pa\bar{3}$ splits into two orbits, Wyckoff positions 9*d* and 3*b*, respectively. Similarly, the S 8*c* orbit of $Pa\bar{3}$ splits into two orbits, Wyckoff positions 18*f* and 6*c*

Table 3
Fractional atomic coordinates of pyrite in $R\bar{3}$, in the two individuals corresponding to CT1 and CT2 twin.

Atom	Coordinates from $Pa\bar{3}$			Coordinates from $Pb\bar{3}$		
Fe1	$\frac{1}{2}$	$\frac{1}{2}$	$\frac{1}{2}$	$\frac{1}{2}$	$\frac{1}{2}$	$\frac{1}{2}$
Fe2	0	0	$\frac{1}{2}$	0	0	$\frac{1}{2}$
S1	0.25659	0.01317	0.62829	0.01317	0.25659	0.37171
S2	$\frac{1}{3}$	$\frac{2}{3}$	0.55155	$\frac{2}{3}$	$\frac{1}{3}$	0.44845

Table 4
FeS_6 coordination polyhedron in untwinned pyrite and at the composition plane of twinned pyrite.

	Untwinned pyrite	CT1 twinned pyrite	CT2 twinned pyrite	Gaubert twin	Relaxed Gaubert twin	Spinel twin	Relaxed Spinel twin
Fe—S bond distances (Å)	6 × 2.263	6 × 2.263	6 × 2.263	6 × 2.263	2 × 2.211 4 × 2.263	6 × 2.263	2 × 2.211 4 × 2.263
S—S bond distances (Å)	1 × 2.160	1 × 2.160	1 × 2.160	1 × 2.160	1 × 2.160	1 × 2.160	1 × 2.160
Shortest S–S nonbonding distances (Å)	1 × 3.077 1 × 3.320	1 × 2.413 1 × 3.077 1 × 3.320	1 × 2.066 1 × 3.077 1 × 3.320	1 × 0.967 1 × 3.077 1 × 3.320	1 × 2.715 1 × 3.077 1 × 3.102 1 × 3.322	1 × 0.967 1 × 2.407 1 × 3.077 1 × 3.320	1 × 2.407 1 × 2.715 1 × 3.077 1 × 3.102 1 × 3.225 1 × 3.320
S—Fe—S angles (°)	3 × 180.00 6 × 85.65 6 × 94.35	1 × 180.00 2 × 148.02 1 × 125.68 4 × 94.35 6 × 85.65 1 × 64.44	1 × 180.00 2 × 148.02 1 × 115.56 6 × 94.35 4 × 85.65 1 × 54.32	1 × 175.58 1 × 149.44 2 × 116.04 2 × 98.70 2 × 94.35 2 × 93.18 4 × 85.65 1 × 24.67	1 × 180.00 1 × 175.58 1 × 149.44 2 × 105.28 2 × 93.18 2 × 92.21 2 × 87.79 2 × 85.65 2 × 74.72	2 × 145.88 1 × 116.39 2 × 116.04 2 × 98.70 2 × 94.35 4 × 85.65 1 × 64.24 1 × 24.67	1 × 180.00 2 × 145.88 1 × 116.39 1 × 105.28 1 × 102.28 2 × 92.21 2 × 87.79 2 × 85.65 2 × 74.72 1 × 64.24

respectively. The two orbits of iron and the S 6*c* orbit fulfil exactly the eigensymmetry $R\bar{3}m$,[2] which is only approximate for the S 18*f* orbit, whose atoms would have to move by 0.623 Å to reach this symmetry (Table 2). Therefore, three of the four orbits are not perturbed by the change of orientation in the twin, while one (S 18*f*) is, and this necessarily results in a distortion of the FeS_6 coordination across the composition plane. To quantitatively estimate this distortion, we show in Table 3 the fractional atomic coordinates in the $Pa\bar{3}$ and $Pb\bar{3}$ settings of the space group, expressed in the coordinate system of the $R\bar{3}$ intersection subgroup, which correspond to the orientation of the two individuals of the twin and in Table 4 the bond distances and angles in the untwinned and twinned sample across the composition plane. Fig. 18 shows the structure of the twinned sample for a composition plane at $z = \frac{1}{2}$ of $R\bar{3}$ setting (grey atoms: iron and S 6*c* orbits, common to both orientations; white and black atoms: S 18*f* orbit, in the two orientations). The distortion of the FeS_6 octahedron is realized through a change in the S—Fe—S angles and the short non-bonding S···S contact (2.4133 Å), much closer to the bonding (2.1599 Å) than to the shortest non-bonding distance (3.0770 Å) in untwinned pyrite (Fig. 19). The situation described in Table 4 and Fig. 19 corresponds to a rigid application of the twin operation: in the twinned sample it is possible to imagine that at the composition plane some relaxation of the structure occurs to reduce the strain, relaxation that is not necessary away from the composition plane, where the change of orientation no longer affects the structure.

[2] The eigensymmetry of iron orbits is actually $Pm\bar{3}m$, a translationengleiche supergroup of $R\bar{3}m$.

4.2. CT2 twin

From the morphological study, the twin operation has been identified as a fourfold rotation about [001], whereas the contact plane is (110). The intersection subgroup is the same

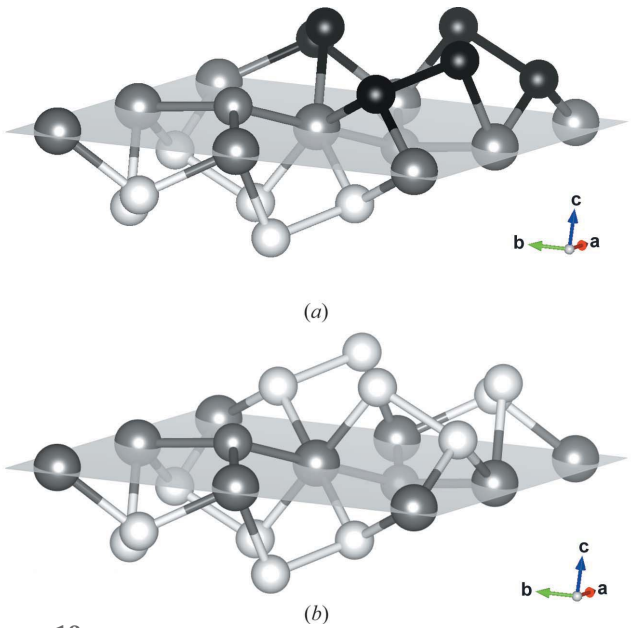

Figure 18
(*a*) The structure of pyrite described in the $R\bar{3}$ setting corresponding to the $\mathcal{G}^*$ intersection subgroup of the space groups of the two individuals of the CT1 twin. Large and small atoms are Fe and S, respectively. Grey atoms are restored by the restoration operation s in equation (8) and occupy therefore equivalent positions in the two orientations. White and black atoms are not restored and occupy therefore non-equivalent positions in the two orientations. The grey plane is the composition plane (001), or (111) in the $Pa\bar{3}$ setting, representing the interface between the two twinned individuals. (*b*) The corresponding view of untwinned pyrite, showing the difference in the coordination of iron across the (001) plane with respect to the twinned structure. This and the following figures drawn with *VESTA* (Momma & Izumi, 2011).

type of group already seen for the CT1 twin, *i.e.* $R\bar{3}$, because both $4_{[001]}$ and $2_{[110]}$ belong to the same twin law, equation (4). The intersection subgroup resulting from the conjugation by $4_{[001]}$ is only conjugated to the intersection subgroup discussed for the CT1 case as the threefold axis that survives is along $[\bar{1}\bar{1}1]$. However, adding a fourfold rotation about [001] would not lead to a group, because, contrary to $\mathcal{H}^*$, no twofold rotation remains in $\mathcal{G}^*$; a 90° rotation about [001] would therefore correspond to an incomplete twin and the fourfold rotation would be a partial operation. We have seen (§3.2) that the composition surface between the two crystals should be the bisector plane (110), which also acts as a twin plane. Adding $m(110)$ to $R\bar{3}$ one gets $R\bar{3}m$, as in the case of CT1; but here the composition plane is $(110)_{Pa\bar{3}} = (110)_{R\bar{3}}$. Indeed, the main difference between CT1 and CT2 twins is the orientation of the composition plane. Fig. 20 shows the structure of the two individuals on the two sides of the composition plane, and Fig. 21 the coordination environment for an iron atom located on that plane. The situation is very similar to that of CT1 twin, but the shortest S···S contact across the composition plane is even shorter, 2.066 Å, *i.e.* in the range for an S—S bond, which could even stabilize the structure on the two sides of the composition plane. This might compensate the angular deformation of the octahedron, which is more pronounced with respect to that in the CT1 twin (Table 4).

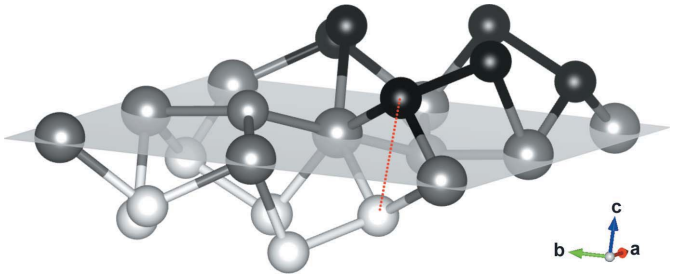

Figure 19
The coordination environment of iron across the composition plane of the CT1 twin. Same conventions as in Fig. 18. The dotted red segment indicates the S···S non-bonding contact is only 2.4133 Å long when the two individuals in the respective orientations are simply juxtaposed one next to the other across the (111) composition plane.

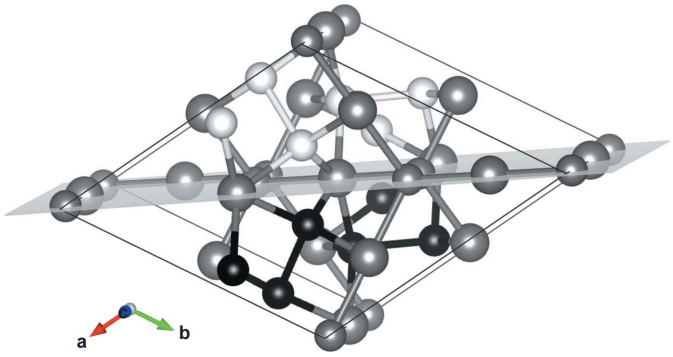

Figure 20
The structure of pyrite describe in the $R\bar{3}$ setting corresponding to the $\mathcal{G}^*$ intersection subgroup of the space groups of the two individuals of the CT2 twin. The grey plane is the composition plane (110), representing the interface between the two twinned individuals.

4.3. Gaubert twin

As seen in (§3.3), in the hexagonal setting of the twin lattice, the composition plane is (001) and the twin operation is a twofold rotation about [120]. The intersection subgroup is $P\bar{3}$. The absence of rhombohedral centring for the twin lattice shows that in this case twinning is by reticular merohedry, with twin index 3. The search for orbits pseudo-symmetry has to be directed toward $P\bar{3}1m$ or $P\bar{3}1c$. No pseudo-symmetry is found in $P\bar{3}1c$ but a significant pseudo-symmetry is instead found in $P\bar{3}1m$ (Table 5). In particular, all the iron atoms at the composition surface (Fe1 and Fe4) are exactly restored by the twin operation. The sulfur atoms closest to the composition surface are S3 and S5, restored within ∼0.48 Å and ∼0.09 Å, respectively (S6, which completes the iron coordination, is

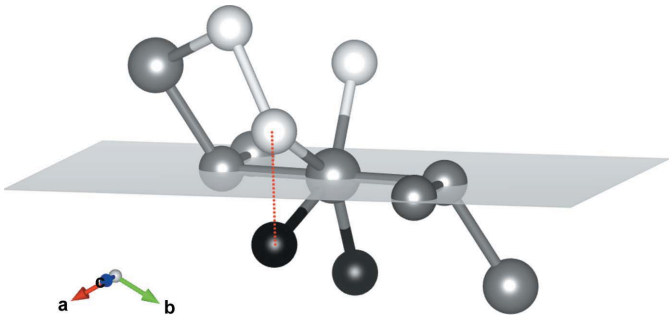

Figure 21
The coordination environment of iron across the composition plane of the CT2 twin. The dotted red segment indicating the S···S non-bonding contact is only 2.066 Å long when the two individuals in the respective orientations are simply juxtaposed one next to the other across the (110) composition plane. This is in the range of an S—S bond; the S···S contact across the composition plane might therefore correspond to a chemical bond, possibly stabilizing the boundary structure.

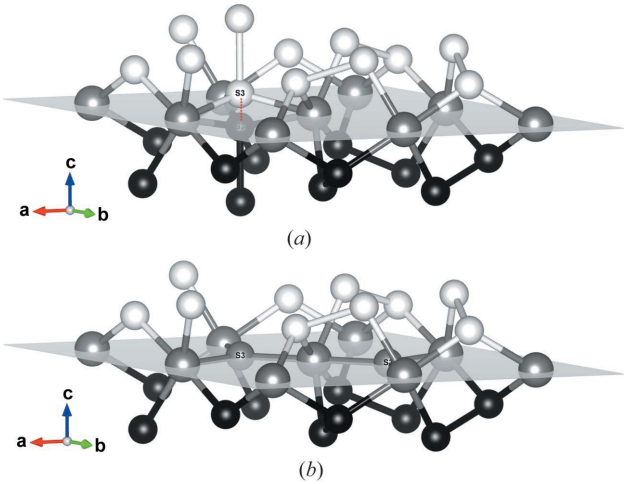

Figure 22
(*a*) The coordination of iron across the (111) composition plane in the Gaubert twin, or (001) when indexed in the coordinate system of the twin lattice. The red dotted segment points out the very short, physically unrealistic S3···S3 contact of 0.967 Å on the two sides on the composition plane. (*b*) In the real twin, the two S3 likely coalesce in an intermediate position, at the composition plane, which restores the coordination environment of iron close to that in the untwinned pyrite, with two out of four Fe-S distance slightly shortened (Table 4).

Table 5
Fractional atomic coordinates of pyrite in $P\bar{3}$, degree of pseudo-symmetry in $P\bar{3}1m$ (Gaubert twin) and in $P6/m$ (spinel twin) measured by $|\mathbf{u}|$.

The covalent radii are the same as in Table 1. The ratio $|\mathbf{u}|/r$ is lower than 1 for all orbits and close to or smaller than 0.5 for several orbits.

Atom	Wyckoff position	Site-symmetry group	Coordinates in $P\bar{3}$			$\lvert\mathbf{u}\rvert$ for $P\bar{3}1m$ **a**, **b**, **c**	$\lvert\mathbf{u}\rvert/r$	$\lvert\mathbf{u}\rvert$ $P6/m$ **a**, **b**, **c**	$\lvert\mathbf{u}\rvert/r$
Fe1	1*a*	$\bar{3}$..	0	0	0	0	0	0	0
Fe2	2*d*	3..	$\frac{1}{3}$	$\frac{2}{3}$	$\frac{1}{3}$	1.1055	0.84	1.1055	0.84
Fe3	6*g*	1	$\frac{2}{3}$	$\frac{1}{3}$	$\frac{1}{3}$	1.1055	0.84	1.1055	0.84
Fe4	3*e*	$\bar{1}$	$\frac{1}{2}$	$\frac{1}{2}$	0	0	0	0	0
S1	2*c*	3..	$\frac{1}{3}$	$\frac{2}{3}$	0.38488	0	0	0	0
S2	2*d*	3..	$\frac{1}{3}$	$\frac{2}{3}$	0.71821	1.0238	0.98	1.0238	0.98
S3	2*d*	3..	$\frac{2}{3}$	$\frac{1}{3}$	0.05155	0.4836	0.46	0.4836	0.46
S4	6*g*	1	0.42325	0.34651	0.53837	0.5090	0.48	0.3599	0.34
S5	6*g*	1	0.75659	0.01317	0.87171	0.0874	0.08	0.6640	0.63
S6	6*g*	1	0.08992	0.67984	0.20504	0.5965	0.57	0.6640	0.63

further away from the composition surface). The coordination polyhedron for iron suffers from significant strain due to the location of S3 rotated 180° about the [001] direction of the twin lattice from its position in the untwinned sample, which leaves iron incompletely coordinated on one side and with two S3 atoms, one from each individual, very close to each other (0.967 Å) [Fig. 22(*a*)]. This is what one obtains by simply juxtaposing the two individuals in the respective orientations, without any structural relaxation. At the formation of this twin, the two positions for S3, at $z = 0.05155$ in one individual, and at $z = -0.05155$ in the second individual, most likely collapse into a single position, at or close to the composition plane, leading to a structural adjustment that is reminiscent of the well known mechanism occurring in the lillianite homologous series through the tropochemical cell-twinning phenomenon (Takéuchi, 1997). The position at $z = 0$ restores the coordination on both sides of iron [Fig. 22(*b*)]; the FeS_6 octahedron at the composition plane presents two slightly short Fe—S bonds (2 × 2.211 Å and 4 × 2.263 Å instead of 6 × 2.263 Å), as well as some deformation of the bond angles (Table 4).

4.4. Does the spinel twin occur in pyrite?

Among common cubic minerals, the spinel twin is well known in fluorite, CaF_2, but exceptional in pyrite. As we have shown, the Gaubert twin is different from the spinel twin, because the twin operation is different, although the composition plane is the same. In the following we apply the struc-

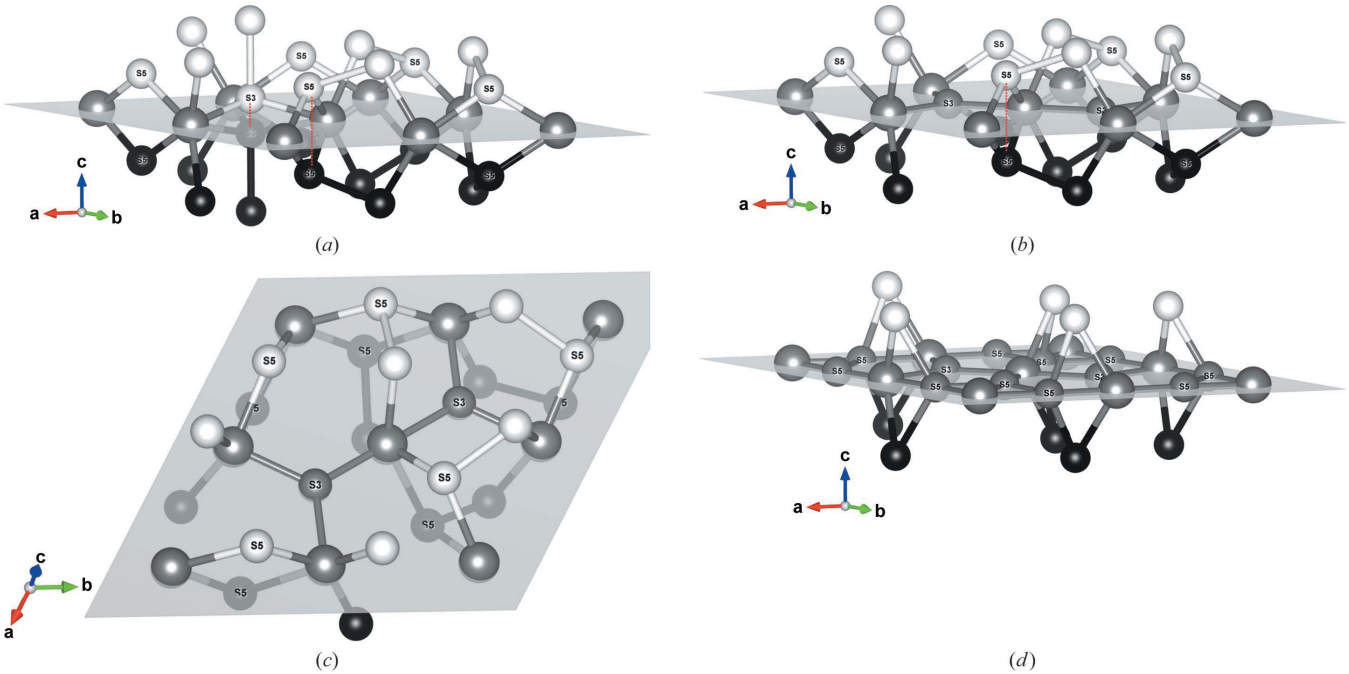

Figure 23
(*a*) The coordination of iron across the (111) composition plane in spinel twin, or (001) when indexed in the coordinate system of the twin lattice. The red dotted segments point out the very short, physically unrealistic S···S contacts on the two sides on the composition plane: 0.967 Å for S3, as in the Gaubert twin, and 2.407 Å for S5···S5. In the real twin, the two S3 likely coalesce in an intermediate position, at the composition plane, but this is not enough to restore the coordination environment of iron, because the S5···S5 contact is still too short (*b*) and because the distribution of sulfur about iron remains non-symmetric (*c*). The same coalescence mechanism for S5 would lead to a totally unrealistic coordination of iron (*d*).

tural analysis to the spinel law, to find possible structural hindrances to its occurrence.

The twin lattice, the composition plane and the intersection subgroup for the spinel twin are the same as for the Gaubert twin. However, the twin operation is different: it is $m_{(001)}$ or $2_{[001]}$, which differ by inversion; the individuals being centrosymmetric, these two operations lead to the same result, *i.e.* they belong to the same twin law. The pseudo-symmetry has to be checked against $P6/m$ or $P6_3/m$, and the results are shown in Table 5. With respect to the Gaubert twin, the restoration of S5, which is the second-nearest sulfur to the composition plane, is much worse, with an S5···S5 contact of 2.407 Å, to be compared with the corresponding distance of 3.172 Å in the Gaubert twin [Fig. 23(*a*)]. The same structural adjustment likely occurring in the Gaubert twin, *i.e.* the coalescence of the two positions for S3 on the composition plane, is not enough to restore the coordination of iron, because the S5···S5 contact is still too short [Fig. 23(*b*)] and because the coordination about iron remains unsymmetrical [Fig. 23(*c*)]. The hypothesis of a similar coalescence for S5 is highly unlikely, because it would lead to an unrealistic coordination for iron [Fig. 23(*d*)]. The distortion at the interface of the spinel twin is therefore much more severe than in the case of the Gaubert twin, which makes the occurrence of the spinel twin in pyrite less probable than the Gaubert twin.

4.5. Iron cross twin

The iron cross twin is a penetration twin for which an irregular composition surface can be expected. A simple overlap of the structure of pyrite in the two orientations (Fig. 24) shows that iron orbits are perfectly restored in the twin, as expected knowing that their eigensymmetry is $Pm\bar{3}m$. The two orientations of the sulfur orbits, on the other hand, correspond to S–S dumbbells rotated by 54°44′, *i.e.* the angle between a ⟨100⟩ direction and the closest ⟨111⟩ direction in a cubic lattice. Depending on the shape and location of the composition surface, one may expect one of the two orientations be actually realized in the twin, or an intermediate orientation, close to the surface.

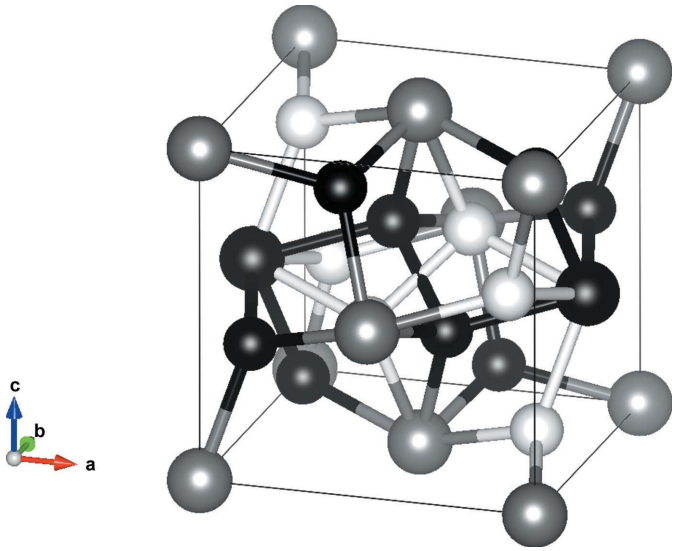

Figure 24
The interpenetration of two pyrite structures rotated by 90° about ⟨001⟩ like in the iron cross penetration twin. The iron atoms are completely restored. The S–S dumbbells in the two orientations (white and black) are rotated by 54°44′, *i.e.* the angle between a ⟨100⟩ direction and the closest ⟨111⟩ direction in a cubic lattice. Depending on the shape and location of the composition surface, one may expect one of the two orientations be actually realized in the twin, or an intermediate orientation, close to the surface.

Rečnik *et al.* (2016), on the basis of atom scale examination of iron cross pyrite through electron microscopy, were able to identify two types of twin boundaries, primary {110} (Cu-rich), and secondary {100} (Cu-free). In the iron cross twin, a strong disorder during pyrite nucleation has probably controlled the appearance of a multiplicity of sub-microscopic twin domains. After that, the growth process favoured the coalescence of domains of the same orientation, leading to parallel growth on the two sides of the composition surface, to result in the final penetration twin between two macro-crystals.

5. Discussion and conclusions

Only one penetration twin ('iron cross') has been confirmed up to now in pyrite, while at least four types of contact twins have been reported. Two are of the merohedric type, where the twin operation is among the symmetry operation of the cubic lattice absent in pyrite structure:

(*a*) Pasto Bueno or CT1 twin by parallel hemitropy: the twin operation is a twofold rotation about a direction ⟨110⟩ contained in the {111} composition plane.

(*b*) V or CT2 reflection twin: the twin operation is a reflection about the twin and composition plane {110}; it also applies to the contact twin from Traversella (Sella, 1858).

(*c*) The Gaubert twin: a twin by parallel hemitropy, where the twin operation is a twofold rotation about a direction $\langle 2\bar{1}\bar{1}\rangle$, contained in the composition plane {111}.

(*d*) Spinel twin: a reflection twin in which the twin operation is a reflection about the twin and composition plane {111}. Without the faces of the pyritohedra, it is hard to differentiate this twin from the Gaubert twin and its existence remains to be proved.

Rečnik *et al.* (2016) have suggested that the occurrence of penetration twins like the iron cross twin be related to the appearance of a multiplicity of sub-microscopic twin domains induced by a strong disorder during pyrite germination. Strunz & Tennyson (1965) suggested that the local structure of (110) twins of pyrite comprises one atomic layer of marcasite, whereas Donnay *et al.* (1977), based on transmission electron microscopy observations, suggested three different interface models.

In contact twins, nucleation is focused on the initiation and stabilization of a single twin boundary. Such a decrease in disorder during the nucleation process may be partly related to a lower temperature, while the appearance of any contact twin may be subordinated to some chemical peculiarities.

Macroscopic examination of contact twins of pyrite is sufficient to understand their twin laws. The structural study

based on the pseudo-symmetry of the crystallographic orbits shows a significant deformation of the FeS_6 coordination polyhedra with respect to untwinned pyrite, which is probably a significant hindrance explaining the rarity of these twins. This interpretation remains to be confirmed by an experimental investigation.

Moëlo (2021) has observed that in fluorite the penetration twin, also known as fluorite twin, involves crystals with cubic habit, whereas in the spinel twin the octahedral habit prevails. These two habits are favoured by, respectively, low and high formation temperatures (Kostov & Kostov, 1999). Because fluorite veins are generally formed discontinuously, at decreasing temperature, a change of habit from octahedral to cubic is observed. This change of habit could result in the modification of a twin originally developed according to the spinel law, more frequent in octahedral crystals, towards the fluorite, typical of cubic crystals.

Pyrite nucleation is kinetically hindered and high supersaturations are required for nucleation to occur (Harmandas *et al.*, 1998). The initial stage of pyrite crystal growth occurs therefore in solutions with large supersaturations: the less stable form, the octahedron, develops first. As pyrite grows, the supersaturation approaches saturation and the most stable (least soluble) form develops, which for pyrite is the cube (Rickard, 2021). The scarcity of spinel twins (whose real existence in pyrite is doubtful) and the confirmed occurrence of iron cross twins is possibly related to a change of habit during crystal growth, from octahedral to cubic, as observed in fluorite. The cause of this morphological modification is however different in the two minerals: a reduction of temperature for fluorite *versus* a reduction is supersaturation in pyrite.

Acknowledgements

We sincerely thank Alain Martaud, French mineral dealer and collector, who selected for us the pyrite twin from Pasto Bueno. Critical remarks by two anonymous reviewers are thankfully acknowledged.

References

Aroyo, M. I., Perez-Mato, J. M., Capillas, C., Kroumova, E., Ivantchev, S., Madariaga, G., Kirov, A. & Wondratschek, H. (2006). *Z. Kristallogr.* **221**, 15–27.
Bravais, A. (1851). *J. Éc. Polytech.* **XX**, 248–276.
Capillas, C., Tasci, E. S., de la Flor, G., Orobengoa, D., Perez-Mato, J. M. & Aroyo, M. I. (2011). *Z. Kristallogr.* **226**, 186–196.
Cordero, B., Gómez, V., Platero-Prats, A. E., Revés, M., Echeverría, J., Cremades, E., Barragán, F. & Alvarez, S. (2008). *Dalton Trans.* **2008**, 2832–2838.
Donnay, G., Donnay, J. D. H. & Iijima, S. (1977). *Acta Cryst.* A**33**, 622–626.
Donnay, J. D. H. & Curien, H. (1960). *Cursillos Conf. Inst. 'Lucas Mallada' CSIC*, **7**, 13–14.
Endo, Y. & Sunagawa, I. (1973). *Am. Mineral.* **58**, 930–935.
Friedel, G. (1904). *Bulletin de la Société de l'Industrie Minérale*, *Quatrième Série*, Tomes III et IV. Saint-Etienne: Société de l'Imprimerie Theolier J. Thomas et C.
Friedel, G. (1926). *Leçons de Cristallographie.* Nancy, Paris, Strasbourg: Berger-Levrault.
Gaubert, P. (1928). *Bull. Soc. Fr. Minéral. Cristallogr.* **51**, 211–212.
Goldschmidt, V. (1920). *Atlas der Kristallformen*, Vol. 6. Heidelberg: Winter.
Goldschmidt, V. & Nicol, W. (1904). *Neues Jahrb. Mineral. Geol. Palaeont.* **2**, 93–113.
Grigor'ev, D. P. (1965). *Ontogeny of Minerals.* Jerusalem: Israel Program for Scientific Translations.
Harmandas, N. G., Navarro Fernandez, E. & Koutsoukos, P. O. (1998). *Langmuir*, **14**, 1250–1255.
Haüy, R. J. (1801). *Traité de Minéralogie*, Tome 1. Paris: Chez Louis.
Kostov, I. & Kostov, R. I. (1999). *Crystal Habits of Minerals. Bulg. Acad. Monogr.* (1), Sofia: Pensoft Publishers.
Marzouki, M. A., Souvignier, B. & Nespolo, M. (2014*a*). *Acta Cryst.* A**70**, 348–353.
Marzouki, M. A., Souvignier, B. & Nespolo, M. (2014*b*). *IUCrJ*, **1**, 39–48.
Moëlo, Y. (2021). *Le Règne Minéral*, **159**, 49–53.
Momma, K. & Izumi, F. (2011). *J. Appl. Cryst.* **44**, 1272–1276.
Nespolo, M. (2015). *Cryst. Res. Technol.* **50**, 362–371.
Nespolo, M. (2019). *Acta Cryst.* A**75**, 551–573.
Nespolo, M. & Ferraris, G. (2006). *Acta Cryst.* A**62**, 336–349.
Nespolo, M. & Moëlo, Y. (2019). *Eur. J. Mineral.* **31**, 785–790.
Nespolo, M., Tokuda, M. & Yoshiasa, A. (2020). *Cryst. Res. Technol.* **55**, 1900063.
Nespolo, M. & Souvignier, B. (2017). *Eur. J. Mineral.* **31**, 939–947.
Palache, C., Berman, H. & Frondel, C. (1944). *Dana's System of Mineralogy*, 7th ed., Vol. 1, *Elements, Sulfides, Sulfosalts, Oxides*. New York: John Wiley & Sons.
Rečnik, A., Zavašnik, J., Jin, L., Čobić, A. & Daneu, N. (2016). *Mineral. Mag.* **80**, 937–948.
Rickard, D. (2021). *Framboids.* Oxford: Oxford University Press.
Rieder, M., Crelling, J. C., Šustai, O., Drábek, M., Weiss, Z. & Klementová, M. (2007). *Int. J. Coal Geol.* **71**, 115–121.
Sella, Q. (1858). *Mem. R. Accad. Sci. Torino 2*, **17**, 337.
Smolař, G. (1913). *Z. Kristallogr.* **52**, 461–500.
Story-Maskelyne, M. (1895). *Crystallography: A Treatise On The Morphology of Crystals.* Oxford: Clarendon Press.
Strunz, H. & Tennyson, Ch. (1965). *Neues J. Miner. Monatsh.* **15**, 247–248.
Takéuchi, Y. (1997). *Tropochemical Cell-Twinning. A Structure Building Mechanism in Crystalline Solids.* Tokyo: Terra Scientific Publishing Company.
Vijayakumar-Syamala, V., Aubert, E., Deutsch, M., Wenger, E., Dhaka, A., Fourmigué, M., Nespolo, M. & Espinosa, E. (2022). *Acta Cryst.* B**78**, 436–449.
Wondratschek, H. (1993). *Mineral. Petrol.* **48**, 87–96.